#### **OPEN ACCESS**



# Repeated Mergers, Mass-gap Black Holes, and Formation of Intermediate-mass Black Holes in Dense Massive Star Clusters

Giacomo Fragione <sup>1,2</sup>, Bence Kocsis <sup>3</sup>, Frederic A. Rasio <sup>1,2</sup>, and Joseph Silk <sup>4,5,6</sup> 

<sup>1</sup> Center for Interdisciplinary Exploration & Research in Astrophysics (CIERA), Evanston, IL 60202, USA 

<sup>2</sup> Department of Physics & Astronomy, Northwestern University, Evanston, IL 60202, USA 

<sup>3</sup> Rudolf Peierls Centre for Theoretical Physics, Clarendon Laboratory, Parks Road, Oxford OX1 3PU, UK 

<sup>4</sup> Institut d'Astrophysique de Paris, UMR7095: CNRS & UPMC, Sorbonne University, Paris, France 

<sup>5</sup> Department of Physics and Astronomy, The Johns Hopkins University, Baltimore, MD, USA 

<sup>6</sup> BIPAC, Department of Physics, University of Oxford, Oxford, UK 

\*\*Received 2021 July 8; revised 2022 January 27; accepted 2022 January 28; published 2022 March 21

#### Abstract

Current theoretical models predict a mass gap with a dearth of stellar black holes (BHs) between roughly  $50\,M_\odot$  and  $100\,M_\odot$ , while above the range accessible through massive star evolution, intermediate-mass BHs (IMBHs) still remain elusive. Repeated mergers of binary BHs, detectable via gravitational-wave emission with the current LIGO/Virgo/Kagra interferometers and future detectors such as LISA or the Einstein Telescope, can form both mass-gap BHs and IMBHs. Here we explore the possibility that mass-gap BHs and IMBHs are born as a result of successive BH mergers in dense star clusters. In particular, nuclear star clusters at the centers of galaxies have deep enough potential wells to retain most of the BH merger products after they receive significant recoil kicks due to anisotropic emission of gravitational radiation. Using for the first time simulations that include full stellar evolution, we show that a massive stellar BH seed can easily grow to  $\sim 10^3 - 10^4\,M_\odot$  as a result of repeated mergers with other smaller BHs. We find that lowering the cluster metallicity leads to larger final BH masses. We also show that the growing BH spin tends to decrease in magnitude with the number of mergers so that a negative correlation exists between the final mass and spin of the resulting IMBHs. Assumptions about the birth spins of stellar BHs affect our results significantly, with low birth spins leading to the production of a larger population of massive BHs.

*Unified Astronomy Thesaurus concepts:* Astrophysical black holes (98); Black holes (162); Intermediate-mass black holes (816); Stellar mass black holes (1611); Gravitational waves (678); Gravitational wave sources (677); Gravitational wave detectors (676); Gravitational wave astronomy (675); Star clusters (1567)

# 1. Introduction

The LIGO/Virgo/KAGRA (LVK) Collaboration has recently released the second Gravitational Wave Transient Catalog (GWTC-2; Abbott et al. 2020a), which, together with results from the first two observing runs (GWTC-1; Abbott et al. 2019), comprises more than 50 events. These detections are transforming our understanding of compact objects and gravitational-wave (GW) physics (Abbott et al. 2020b, 2020c). Over the coming years and decades, current (LIGO, Virgo, and KAGRA) and future (e.g., LISA, the Einstein Telescope, and DECIGO) GW detectors promise to provide an unprecedented number of detections of black holes (BHs) and neutron stars (NSs).

The origin of binary mergers is still highly uncertain, with several possible scenarios that could potentially account for most of the observed events. These include mergers from isolated binary star evolution (e.g., Dominik et al. 2013; Belczynski et al. 2016; de Mink & Mandel 2016; Chruslinska et al. 2018; Giacobbo & Mapelli 2018; Spera et al. 2019; Breivik et al. 2020; Bavera et al. 2021; Santoliquido et al. 2021; Tanikawa et al. 2021), dynamical formation in dense star clusters (e.g., Portegies Zwart & McMillan 2000; Askar et al. 2017; Banerjee 2018; Fragione & Kocsis 2018; Kremer et al. 2018, 2019; Rodriguez et al. 2018, 2020; Samsing et al. 2018; Hamers & Samsing 2019;

Original content from this work may be used under the terms of the Creative Commons Attribution 4.0 licence. Any further distribution of this work must maintain attribution to the author(s) and the title of the work, journal citation and DOI.

Rastello et al. 2019; Antonini & Gieles 2020; Di Carlo et al. 2020; Fragione & Banerjee 2020; Fragione & Loeb 2021), mergers in triple and quadruple systems (e.g., Antonini & Perets 2012; Arca-Sedda et al. 2021; Grishin et al. 2018; Liu & Lai 2018, 2019; Rodriguez & Antonini 2018; Fragione & Kocsis 2019; Fragione et al. 2019a, 2019b, 2020; Martinez et al. 2020; Hamers et al. 2021), and mergers of compact binaries in galactic nuclei (e.g., O'Leary et al. 2009; Bartos et al. 2017; Petrovich & Antonini 2017; Stone et al. 2017b; Arca-Sedda & Gualandris 2018; Hamers et al. 2018; Hoang et al. 2018; Fragione et al. 2019b; Liu et al. 2019; Rasskazov & Kocsis 2019; Gondán & Kocsis 2020; McKernan et al. 2020; Tagawa et al. 2020a; Wang et al. 2021). While several formation scenarios can account for some or even all of the merger rate, the contribution of different channels will hopefully be disentangled using a combination of the mass, spin, redshift, and eccentricity distributions as the number of detected events increases (e.g., O'Leary et al. 2009; Gondán et al. 2018; Perna et al. 2019; Arca Sedda et al. 2020; Martinez et al. 2021; Su et al. 2021; Tagawa et al. 2021b, 2021c; Wong et al. 2021; Zevin et al. 2021).

One of the most interesting events in GWTC-2 is GW190521, a binary black hole (BBH) consistent with the merger of two BHs with masses of  $91.4^{+29.3}_{-17.5}\,M_{\odot}$  and  $66.9^{+15.5}_{-9.2}\,M_{\odot}$  (The LIGO Scientific Collaboration, & the Virgo Collaboration 2020a, 2020b). Stellar evolutionary models predict no BHs with masses larger than about 50– $70\,M_{\odot}$  (high-mass gap), resulting from the pulsational pair-instability process that affects massive progenitors. Whenever the preexplosion stellar core is in the range

45–65  $M_{\odot}$ , large amounts of mass can be ejected, leaving a BH remnant with a maximum mass of around 50–70  $M_{\odot}$  (Heger et al. 2003; Woosley 2017). Recent studies have shown that the exact lower boundary of the high-mass gap depends on the stellar metallicity (Woosley 2017; Limongi & Chieffi 2018; Belczynski et al. 2020; Vink et al. 2021); the upper boundary is around 125  $M_{\odot}$  whenever the metallicity is ≤  $10^{-3}$  (Spera & Mapelli 2017; Renzo et al. 2020).

BHs more massive than the limit imposed by the pulsational pair instability can be produced dynamically in the core of a dense star cluster. Here, three- and four-body interactions can catalyze the growth of a BH seed through repeated mergers with smaller BHs (e.g., Gültekin et al. 2004; Antonini et al. 2019; Baibhay et al. 2020; Fragione & Silk 2020; Mapelli et al. 2021). A fundamental limit for hierarchical mergers comes from the recoil kick imparted to merger remnants (e.g., Lousto et al. 2010; Lousto & Zlochower 2011; Varma et al. 2019). Depending on the mass ratio and the spins of the merging BHs, the recoil kick can be as high as  $\sim 100-1000 \,\mathrm{km \, s^{-1}}$  and could result in the ejection of the merger remnant if it exceeds the local escape speed. However, if the host cluster hosts a supermassive black hole (SMBH), or if the cluster does not have an SMBH but it is massive and dense enough, as in nuclear star clusters (NSCs) or the most massive globular clusters (GCs), hierarchical mergers can build up BHs in the mass gap and even form intermediate-mass black holes (IMBHs), possibly explaining the formation of GW19052-like events (e.g., Antonini & Gieles 2020; Fragione & Silk 2020; Fragione et al. 2020; Baibhav et al. 2021; Mapelli et al. 2021; Tagawa et al. 2021a, 2021c).

While interesting, repeated mergers are computationally expensive to investigate in detail and over broad ranges of initial conditions with full N-body simulations (e.g., Aarseth 2003; Giersz 2006; Pattabiraman et al. 2013). Therefore, developing an alternative and more rapid method is highly desirable. In this paper, we present a semianalytic framework to investigate hierarchical mergers in dense star clusters, which expands upon the method originally developed in Fragione & Silk (2020). Our approach allows us to rapidly probe how the outcomes of hierarchical mergers in dense star clusters are affected by cluster masses, stellar densities, and metallicities and by different assumptions on the BH-mass spectrum and spins. Importantly, we have also integrated for the first time the updated versions of the stellar evolution codes SSE and BSE (Hurley et al. 2000, 2002), including the most up-to-date prescriptions for stellar winds and compact object formation (Banerjee et al. 2020). This provides more realistic BH-mass spectra and spins and allows us to study the role of primordial

This paper is organized as follows. In Section 2, we discuss our numerical method to study repeated mergers, the formation of IMBHs, and BH mergers in the mass gap. In Section 3, we discuss the assembly of massive BHs through repeated mergers and study the role of the cluster metallicity, primordial binary fraction, and prescriptions for the remnant spin. Finally, in Section 4, we discuss the implications of our results and draw our conclusions.

#### 2. Method

In what follows, we describe the details of the numerical method we use to follow the evolution of a BH of seed mass  $\mathcal{M}$ , which undergoes mergers with other BHs. In Table 1, we

 Table 1

 Description of Important Quantities Used in the Text

Symbol	Description					
$M_{\rm CL}$	Cluster mass					
$\rho_{\rm CL}$	Cluster-mass density					
$\rho_{ m BH}$	BH-mass density					
$n_{\rm CL}$	Cluster number density					
$n_{\mathrm{BH}}$	BH number density					
$Z_{\rm CL}$	Cluster metallicity					
$v_{ m esc}$	Cluster escape speed					
$\sigma$	Cluster velocity dispersion					
$\sigma_{\rm BH}$	BH velocity dispersion					
<i>f</i> вн	Fraction of the cluster mass in BHs					
$\mathcal{M}$	Mass of the growing BH					
$\mathcal{M}_*$	Mass of the stellar progenitor of the BH seed					
$\mathcal{M}_{ ext{ini}}$	Mass of the BH seed					
$\beta_*$	Slope of stellar initial mass function for $m_* > 0.5  M_\odot$					
$m_{\min,*}$	Minimum mass of the stellar-mass function					
$m_{\text{max},*}$	Maximum mass of the stellar-mass function					
$f_{\mathrm{b},*}$	Primordial binary fraction for massive stars $(m_* > 20 M_{\odot})$					
$q_*$	Mass ratio of the primordial stellar binary					
$a_*$	Semimajor axis of the primordial stellar binary					
$a_{\min,*}$	Minimum semimajor axis of the primordial stellar binary					
$a_{\max,*}$	Maximum semimajor axis of the primordial stellar binary					
$a_{h,*}$	Hard-soft boundary for the primordial stellar binary					
$e_*$	Eccentricity of the primordial stellar binary					
$v_{\rm natal}$	Natal kick imparted at BH formation					
$\nu$	Velocity dispersion of the Maxwellian distribution of natal kicks					
χ	BH dimensionless spin parameter					
Χм	Spin parameter of BH seed					
$m_{ m min,BH}$	Minimum mass of the BH-mass function					
$m_{ m max,BH}$	Maximum mass of the BH-mass function					
$\beta_{\rm BH}$	Slope of the BH-mass function					
$a_{\rm ej}$	Semimajor axis of the BH binary corresponding to ejection from the parent cluster					
$a_{\rm GW}$	Semimajor axis of the BH binary when GW emission takes over					
$e_{ m BH}$	Eccentricity of the BH binary					
$\tau_{\mathrm{DF},*}$	Dynamical friction timescale for the BH seed progenitor					
$ au_{ m DF}$	Dynamical friction timescale for the BH seed					
$ au_{3\mathrm{bb}}$	Timescale for binary formation via three-body interaction					
$\tau_1^*$	Timescale for binary formation via binary–single interaction mediated by stellar binaries					
$ au_1$	Timescale for binary formation via binary-single interaction					
$ au_2$	Timescale to shrink the BH binary to $max(a_{ej}, a_{GW})$					
$ au_{\mathrm{GW}}$	Timescale to merge via GW emission					
$v_{\rm kick}$	Recoil kick due to anisotropic GW emission					
$\mathcal{M}_{\mathrm{fin}}$	Mass of the merger remnant					

summarise the notation of the most important quantities referenced to in this paper.

# 2.1. Cluster Properties

The characteristics of the host NSC are essentially determined by its mass  $M_{\rm CL}$ , its half-mass radius  $r_{\rm h}$ , and core radius  $r_{\rm c}$ . We assume that the cluster density is described by a three-parameter potential-density pair described in Stone & Ostriker (2015),

$$\rho_{\rm CL} = \frac{\rho_{\rm c}}{(1 + r^2/r_{\rm c}^2)(1 + r^2/r_{\rm h}^2)},\tag{1}$$

where

$$\rho_{\rm c} = \frac{M_{\rm CL}(r_{\rm h} + r_{\rm c})}{2\pi^2 r_{\rm c}^2 r_{\rm h}^2} \tag{2}$$

is the central density,  $r_{\rm c}$  is the core radius, and  $r_{\rm h}$  is the half-mass density radius when  $r_{\rm h} \gg r_{\rm c}$ . These models are designed as an analytically tractable alternative to single-mass King models. The escape velocity from the center is<sup>7</sup>

$$v_{\rm esc} = 2\sqrt{\frac{\log(r_{\rm h}/r_{\rm c})}{\pi}} \left(\frac{GM_{\rm CL}}{r_{\rm h} - r_{\rm c}}\right)^{1/2}$$

$$\approx 50 \text{ km s}^{-1} \left(\frac{M_{\rm CL}}{10^5 M_{\odot}}\right)^{1/2} \left(\frac{r_h}{1 \text{ pc}}\right)^{-1/2}, \tag{3}$$

and the core velocity dispersion is computed as

$$\sigma = \frac{3(\pi^2 - 8)}{8} v_{\text{esc}}.\tag{4}$$

Finally, the cluster metallicity,  $Z_{\rm CL}$ , determines the BH-mass spectrum. The velocity dispersion and densities of BHs in the core can be related to the corresponding quantities for the background stars. Stellar and BH velocity dispersions are related by

$$\xi^{-2} = \frac{\langle m_{\rm BH} \rangle \sigma_{\rm BH}^2}{\langle m_* \rangle \sigma^2},\tag{5}$$

where  $\langle m_* \rangle \approx 0.5\,M_\odot$  and  $\langle m_{\rm BH} \rangle \approx 10\,M_\odot$ , which quantifies the deviation from energy equipartition between stars and BHs. We fix  $\xi=1/\sqrt{5}$ , which gives timescales for BBH formation consistent with the numerical study of Morscher et al. (2015). When the BH population dominates the mass in the core, its density is (Lee 1995; Choksi et al. 2019)

$$\rho_{\rm BH} = \frac{1}{2} \left( \frac{r_{\rm c}}{r_{\rm h}} \right)^2 f_{\rm BH}^{-2} \ \rho_{\rm c} \approx \frac{f_{\rm BH}^{-2}}{4\pi^2} \frac{M_{\rm CL}}{r_{\rm h}^3},\tag{6}$$

where  $f_{\rm BH} = 0.01$  is the fraction of the cluster mass in BHs.

Note that we assume that the masses and sizes of NSCs do not evolve significantly during their lifetime. Observations show that NSCs in general tend to have a wide range of stellar ages, including young stellar populations (e.g., Rossa et al. 2006; Seth et al. 2006). Indeed, star clusters lose mass, expand as a consequence of two-body relaxation, are continuously supplied with stars and gas from the rest of the galaxy, and accrete star clusters. For a more detailed discussion of the possible effects of NSC evolution, see Section 4.

# 2.2. Population of Nuclear Star Clusters

To generate a population of NSCs, we start by sampling galaxy masses from a Schechter function:

$$\Phi(M_{*,\mathrm{gal}}) \propto \left(\frac{M_{*,\mathrm{gal}}}{M_{\mathrm{c}}}\right)^{\alpha_{\mathrm{c}}} \exp\left(-\frac{M_{*,\mathrm{gal}}}{M_{\mathrm{c}}}\right),$$
(7)

where  $M_{*,\rm gal}$  is the stellar mass of a given galaxy. We set  $M_{\rm c}=10^{11.14}\,M_{\odot}$  and  $\alpha_{\rm c}=1.43$ , as extracted from the EAGLE cosmological simulations in Furlong et al. (2015). We then use

scaling relations for late-type galaxies from Georgiev et al. (2016) to scale the galaxy mass to the NSC mass,

$$\log(M_{\rm CL}/c_1) = \zeta \times \log(M_{*,\rm gal}/c_2) + \psi, \tag{8}$$

and to draw the half-mass radius

$$\log(r_{\rm h}/c_3) = \kappa \times \log(M_{\rm CL}/c_4) + \omega, \tag{9}$$

where  $c_1 = 2.78 \times 10^6 \, M_{\odot}$ ,  $c_2 = 3.94 \times 10^9 \, M_{\odot}$ ,  $\zeta = 1.001^{+0.054}_{-0.067}$ ,  $\psi = 0.016^{+0.023}_{-0.061}$ , and  $c_3 = 3.31$  pc,  $c_4 = 3.60 \times 10^6 \, M_{\odot}$ ,  $\kappa = 0.321^{+0.047}_{-0.038}$ ,  $\omega = -0.011^{+0.014}_{-0.031}$ . In sampling from Equations (8)–(9), we consider the scatter in the fit parameters.

#### 2.3. Black Hole Seeds

To compute the initial BH seed mass  $\mathcal{M}_{ini}$ , we first sample the mass of its stellar progenitor,  $\mathcal{M}_*$ , from the canonical initial mass function (Kroupa 2001),

$$\xi(m_*) = k_1 \begin{cases} \left(\frac{m_*}{0.5}\right)^{-1.3} & 0.08 \leqslant m_*/M_{\odot} \leqslant 0.50, \\ \left(\frac{m_*}{0.5}\right)^{-\beta_*} & 0.50 \leqslant m_*/M_{\odot} \leqslant 150.0, \end{cases}$$
(10)

where  $k_1 \approx 0.62$  is a normalization factor for  $\beta_* = 2.35$ . The mass of the BH seed progenitor is drawn from the range  $[m_{\min,*}, m_{\max,*}]$ , where  $m_{\min,*} = 20~M_{\odot}$  and  $m_{\max,*} = 150~M_{\odot}$ , respectively, which roughly encompass the possible masses of BH progenitors. We then evolve the progenitor mass  $\mathcal{M}_*$  at a metallicity  $Z_{\text{CL}}$  using the stellar evolution code SSE (Hurley et al. 2000). Our current version of SSE includes the most up-to-date prescriptions for stellar winds and remnant formation (see Banerjee et al. 2020 and references therein). Alternatively, the initial BH seed mass  $\mathcal{M}_{\text{ini}}$  can be fixed to a specific value. One possibility is that the initial BH seed is the result of runaway growth, and its mass is typically  $\lesssim 1\%$  of the cluster mass (Portegies Zwart & McMillan 2002).

If the primordial binary fraction in high-mass stars,  $f_{b_*}$ , is sufficiently high, the stellar progenitor,  $\mathcal{M}_*$ , can be born in a binary system. In this case, we sample the mass of the companion using a uniform distribution in the mass ratio  $q_*$ , consistent with observations of massive binary stars (Sana et al. 2012; Duchêne & Kraus 2013; Sana 2017):

$$f(q_*) \propto \text{const.}$$
 (11)

We draw the semimajor axis  $a_*$  using a log-uniform distribution, roughly consistent with the observational study of Kobulnicky et al. (2014),

$$f(a_*) \propto \frac{1}{a_*} \,, \tag{12}$$

in the range [ $a_{\min}$ ,  $a_{\max}$ ]. We fix the minimum semimajor axis to 0.1 au, while the maximum semimajor axis is set to be the hard–soft boundary, defined as

$$a_h = 800 \text{ au} \left( \frac{g_* \mathcal{M}_*^2}{400 \, M_\odot^2} \right) \left( \frac{\sigma}{30 \, \text{km s}^{-1}} \right)^{-2}.$$
 (13)

Finally, we sample the binary eccentricity,  $e_*$ , from a thermal distribution (Heggie 1975).

The primordial binary is then evolved using BSE (Hurley et al. 2002), which includes the most up-to-date prescriptions

 $<sup>^{7}</sup>$  We assume an average compactness parameter  $r_{\rm h}/r_{\rm c}=10$  (Georgiev & Böker 2014).

for stellar winds and remnant formation (see Banerjee et al. 2020 and references therein). There are three possible outcomes of binary stellar evolution: (i) the binary components merge, (ii) a binary BH is formed, and (iii) the binary disrupts as a result of stellar evolution and/or natal kicks, which we assume are imparted to the compact object remnant when the progenitor star collapses due to mass loss and supernova explosion. For simplicity, we only consider primordial binaries that lead to the formation of a binary BH. Note, however, that recent results have shown that subsequent mergers catalyzed by massive binaries can produce massive BHs in the early phases of the cluster evolution (Kremer et al. 2020a; González et al. 2021). At the moment, we do not model this scenario, which we leave to a future study. We take the natal kick to follow a Maxwellian distribution,

$$p(v_{\text{natal}}) \propto v_{\text{natal}}^2 e^{-v_{\text{natal}}^2/\nu^2},$$
 (14)

with velocity dispersion  $\nu = 265 \, \mathrm{km \, s^{-1}}$ , based on observations of radio pulsars (Hobbs et al. 2005). BH natal kicks are assigned assuming momentum conservation (Fryer & Kalogera 2001); thus, the natal velocity of a BH of mass  $m_{\mathrm{BH}}$  is lowered by a factor of 1.4  $M_{\odot}/m_{\mathrm{BH}}$ , with 1.4  $M_{\odot}$  being the typical neutron star mass. Aside from unbinding the binary, natal kicks can eject the BH seed, either as a single or in a binary, from the parent cluster whenever they exceed the cluster escape speed. For what concerns the BH natal spins  $\chi$ , we consider two different models, where the prescriptions of the GENEVA stellar evolution code (Eggenberger et al. 2008; Ekström et al. 2012) and MESA stellar evolution code (Paxton et al. 2011, 2015) are used, respectively. Alternatively, the initial spin of BHs is assumed to vanish, consistent with the recent findings of Fuller & Ma (2019).

# 2.4. Dynamical Interactions and Mergers

Whether the progenitor is born as a single or in a binary star, it sinks to the cluster center from its initial position via dynamical friction over a timescale (Chandrasekhar 1943)

$$\tau_{\rm df} \approx 17 \text{ Myr} \left( \frac{20 \, M_{\odot}}{(1 + q_*) \, M_*} \right) \left( \frac{\mathcal{R}}{1 \text{ pc}} \right)^{3/2} \left( \frac{M_{\rm CL}}{10^5 \, M_{\odot}} \right)^{1/2}, (15)$$

where  $\mathcal{R}$  is the distance from the cluster center. In the previous equation,  $q_*=0$  in the case where the seed progenitor is a single. As a typical initial distance, we choose  $r_{\rm h}$ , such that the initial dynamical friction timescale is  $\tau_{\rm df}(r_{\rm h})$ . As discussed, compact objects are imparted a natal kick that could eject them from the core of the parent cluster. Therefore, we check that the natal kicks imparted to the system are below the cluster escape speed,  $v_{\rm esc}$ . If not ejected from the cluster, the system sinks back to the cluster center over a dynamical friction timescale.

In the case where the BH seed was born with a companion, stellar evolution and natal kicks can unbind the binary, leaving the BH seed as a single. In the case where the binary remains bound, the stellar evolutionary processes could produce a binary BH, whose semimajor axis exceeds the hard–soft boundary (see Equation (13)). Any interaction with a third BH or star will tend to make the binary even softer and, eventually, disrupt it, leaving two single BHs (Heggie 1975). In these cases, where we simply keep following the further evolution of the most massive BH, or in the case where the BH seed was

born as a single star, a new BH companion can be found in the core of the dense cluster via dynamical friction. The mass of  $m_2$  is drawn assuming that the pairing probability scales as  $\mathcal{P} \propto (\mathcal{M} + m_2)^{\beta_{\rm BH}}$ . We set  $\beta_{\rm BH} = 4$ , based on numerical simulations of globular clusters (O'Leary et al. 2016), and sample the secondary mass in the range  $[m_{\rm min,BH}, m_{\rm max,BH}]$ , as appropriate for the BH-mass spectrum at metallicity  $Z_{\rm CL}$ .

Interactions to form a binary BH come in two flavors: encounters between three single objects and encounters between a single and a binary. The typical timescale for the former is (e.g., Lee 1995)

$$\tau_{3bb} = 125 \text{ Myr} \left( \frac{10^6 \text{ pc}^{-3}}{n_{\text{BH}}} \right)^2 \times \left( \xi^{-1} \frac{\sigma}{30 \text{ km s}^{-1}} \right)^9 \left( \frac{20 M_{\odot}}{\mathcal{M}} \right)^5, \tag{16}$$

where  $n_{\rm BH} = \rho_{\rm BH}/\langle m_{\rm BH}\rangle$  is the number density of BHs near the center. Formation of BBHs via exchange binary–single encounters are first mediated by stellar binaries, which, assuming an overall stellar binary fraction of 0.05, happen over a timescale (Antonini & Rasio 2016)

$$\tau_{1}^{*} = 220 \text{ Myr} \left( \frac{10^{6} \text{ pc}^{-3}}{n_{c}} \right) \left( \frac{\sigma}{30 \text{ km s}^{-1}} \right) \times \left( \frac{20 M_{\odot}}{\mathcal{M} + 2m_{*}} \right) \left( \frac{1 \text{ au}}{a_{h}^{*}} \right), \tag{17}$$

where  $n_{\rm c}=\rho_{\rm c}/\langle m_* \rangle$  is the stellar number density near the center and

$$a_h^* = 2 \operatorname{au} \left( \frac{m_*}{1 \, M_\odot} \right)^2 \left( \frac{\sigma}{30 \, \text{km s}^{-1}} \right)^{-2}$$
 (18)

is the hard–soft semimajor axis for a stellar binary. In our calculation, we assume  $m_* = 0.5~M_{\odot}$ . Once BH binaries are formed, they dominate the dynamics inside the cluster core and, assuming a BH binary fraction of 0.01 (Morscher et al. 2015), binary–single encounters between a single BH and a BH binary occur on a timescale (Miller & Lauburg 2009; Antonini & Rasio 2016)

$$\tau_{\rm l} = 450 \text{ Myr } \xi^{-1} \left( \frac{10^6 \text{ pc}^{-3}}{n_{\rm BH}} \right) \left( \frac{\sigma}{30 \text{ km s}^{-1}} \right) \times \left( \frac{20 M_{\odot}}{m_3 + \mathcal{M} + m_2} \right) \left( \frac{1 \text{ au}}{a_h} \right), \tag{19}$$

where  $m_3$  is the mass of the third BH taking part in the interaction, which we set to  $10 M_{\odot}$  in our calculations.

We then compute the further evolution of a binary BH that is dynamically assembled or that originates from a primordial stellar binary (not unbound by stellar evolution or natal kicks). We assume that the BH binary shrinks at a constant rate (see Equation (24)), eventually to the regime where GWs take over (Quinlan 1996). During any of the interactions, the binary could receive a recoil kick high enough to be ejected, which happens when (Antonini & Rasio 2016)

$$a_{\rm ej} > a_{\rm GW},$$
 (20)

where

$$a_{\rm ej} = 0.2 \text{ au} \left( \frac{400 M_{\odot}^2}{(\mathcal{M} + m_2)(m_3 + \mathcal{M} + m_2)} \right) \times \left( \frac{\mu}{10 M_{\odot}} \right) \left( \frac{50 \text{ km s}^{-1}}{v_{\rm esc}} \right)^2, \tag{21}$$

with  $\mu$  being the reduced mass of the  $\mathcal{M}-m_2$  system, and

$$a_{\rm GW} = 0.08 \text{ au} \left(\frac{\mathcal{M} + m_2}{20 M_{\odot}}\right)^{3/5} \left(\frac{10^5 M_{\odot} \text{ pc}^{-3}}{\rho_{\rm BH}}\right)^{1/5} \times \left(\frac{\sigma}{30 \text{ km s}^{-1}}\right)^{1/5} \left(\frac{q}{(1+q)^2}\right)^{1/5}, \tag{22}$$

with  $q = m_2/\mathcal{M}$ . Assuming that each interaction removes a fraction  $0.2m_3/(\mathcal{M} + m_2)$  of the binary-binding energy (Quinlan 1996), the binary will shrink until reaching  $\max(a_{\rm ej}, a_{\rm GW})$  over a timescale (Miller & Hamilton 2002)

$$\tau_2 \approx 5 \left( \frac{m_3}{\mathcal{M} + m_2} \right)^{-1} \tau_{21},$$
(23)

where

$$\tau_{21} = 20 \text{ Myr } \xi^{-1} \left( \frac{10^6 \text{ pc}^{-3}}{n_{\text{BH}}} \right) \left( \frac{\sigma}{30 \text{ km s}^{-1}} \right) \times \left( \frac{0.05 \text{ au}}{\text{max}(a_{\text{ej}}, a_{\text{GW}})} \right) \left( \frac{20 M_{\odot}}{\mathcal{M} + m_2} \right).$$
 (24)

We sample all the relevant timescales from a Poisson distribution, that is,  $\exp(-t/\Theta)$ . In particular,  $\Theta = \min(\tau_{3\text{bb}}, \tau_1)$  is the mean time after which the seed forms a BBH, while  $\Theta = \tau_2$  is the mean time after which the BBH shrinks to  $\max(a_{\text{ej}}, a_{\text{GW}})$ . Finally, the binary merges over a timescale (Peters 1964)

$$\tau_{\text{GW}} = 250 \text{ Myr} \left( \frac{8000 \, M_{\odot}}{\mathcal{M} m_2 (\mathcal{M} + m_2)} \right) \times \left( \frac{\max(a_{\text{ej}}, a_{\text{GW}})}{0.05 \, \text{au}} \right)^4 (1 - e_{\text{BH}}^2)^{7/2}, \tag{25}$$

where  $e_{\rm BH}$  is the eccentricity, which we sample from a thermal distribution (Jeans 1919; Heggie 1975). If  $a_{\rm ej} > a_{\rm GW}$ , the binary is ejected from the cluster, halting further growth, otherwise the merger happens in the cluster.

# 2.5. Recoil Kicks and Merger Remnants

The merger remnant receives a recoil kick as a result of the anisotropic emission of GWs at merger and can be ejected from the host star cluster. This GW recoil kick depends on the asymmetric mass ratio  $\eta = q/(1+q)^2$  and on the magnitude of the dimensionless spin parameters  $|\chi_1| = |\chi_{\mathcal{M}}|$  and  $|\chi_2|$ . In our models, spin orientations are assumed to be isotropic, as appropriate for merging binaries assembled dynamically. We model the recoil kick as (Lousto et al. 2010, 2012)

$$\mathbf{v}_{\text{kick}} = \mathbf{v}_m \hat{\mathbf{e}}_{\perp,1} + \mathbf{v}_{\parallel} (\cos \xi \hat{\mathbf{e}}_{\perp,1} + \sin \xi \hat{\mathbf{e}}_{\perp,2}) + \mathbf{v}_{\parallel} \hat{\mathbf{e}}_{\parallel}, \tag{26}$$

where

$$v_m = A\eta^2 \sqrt{1 - 4\eta} \left( 1 + B\eta \right) \tag{27}$$

$$v_{\perp} = \frac{H\eta^2}{1+q} (\chi_{2,\parallel} - q\chi_{1,\parallel})$$
 (28)

$$v_{\parallel} = \frac{16\eta^{2}}{1+q} [V_{1,1} + V_{A}\tilde{S}_{\parallel} + V_{B}\tilde{S}_{\parallel}^{2} + V_{C}\tilde{S}_{\parallel}^{3}] \times |\chi_{2,\perp} - q\chi_{1,\perp}|\cos(\phi_{\Delta} - \phi_{1}).$$
 (29)

The  $\perp$  and  $\parallel$  refer to the direction perpendicular and parallel to the orbital angular momentum, respectively, while  $\hat{e}_{\parallel,1}$  and  $\hat{e}_{\parallel,2}$  are orthogonal unit vectors in the orbital plane. We have also defined the vector

$$\tilde{S} = 2\frac{\chi_2 + q^2 \chi_1}{(1+q)^2},\tag{30}$$

 $\phi_1$  as the phase angle of the binary, and  $\phi_\Delta$  as the angle between the in-plane component of the vector,

$$\Delta = M^2 \frac{\chi_2 - q\chi_1}{1+q},\tag{31}$$

and the infall direction at merger. Finally, we adopt  $A = 1.2 \times 10^4$  km s<sup>-1</sup>,  $H = 6.9 \times 10^3$  km s<sup>-1</sup>, B = -0.93,  $\xi = 145^\circ$  (González et al. 2007; Lousto & Zlochower 2008), and  $V_{1,1} = 3678$  km s<sup>-1</sup>,  $V_A = 2481$  km s<sup>-1</sup>,  $V_B = 1793$  km s<sup>-1</sup>, and  $V_C = 1507$  km s<sup>-1</sup> (Lousto et al. 2012). We adjust the final total spin of the merger product,  $\chi_{\text{fin}}$ , and its mass,  $\mathcal{M}_{\text{fin}}$ , using the results of Jiménez-Forteza et al. (2017), which we generalized to precessing spins using an approach similar to Hofmann et al. (2016).

Whenever  $v_{\rm kick} > v_{\rm esc}$ , the remnant is ejected from the host cluster, while, if  $v_{\rm kick} < v_{\rm esc}$ ,  $\mathcal{M}$  will be retained. After a dynamical friction timescale (see Equation (15)), the merged remnant sinks back to the center, eventually forming new binaries and merging, further growing in mass.

# 2.6. Overview of the Method and Growth of a Black Hole Seed

We summarize the various steps of our method, which allow us to study the evolution and growth of a black hole seed.

- 1. We sample the stellar mass of the seed progenitor,  $\mathcal{M}_*$ , from Equation (10). To decide whether the seed progenitor was born in a binary system, we extract a random number. If it is smaller than  $f_{b,*}$ , we sample the companion mass (Equation (11)) and the orbital properties of the binary. Finally, we compute the timescale for the seed to sink to the cluster center (Equation (15)).
- 2. We evolve the seed progenitor using SSE, if it is a single, or using BSE, if it is in a binary. If the seed is not ejected by natal kicks (Equation (14)), we compute the timescale for the seed to sink back to the cluster center (Equation (15)).
- 3. In the case where the BH seed,  $\mathcal{M}$ , is a single or the primordial binary and is disrupted as a result of stellar evolution, leaving behind a single BH, we compute the timescale (Equations (16)–(19)) to find a BH companion. The mass of the companion,  $m_2$ , is drawn assuming that the pairing probability scales as  $\mathcal{P} \propto (\mathcal{M} + m_2)^4$ .
- 4. After the BBH is formed, or in the case where the BBH is the result of the binary stellar evolution of the primordial binary, we compute the timescale (Equation (24)) for it to shrink to  $\max(a_{ej}, a_{GW})$ .
- 5. If  $a_{\rm ej} > a_{\rm GW}$ , the BBH is ejected from the cluster, halting further growth. If  $a_{\rm ej} < a_{\rm GW}$ , we compute the timescale to merge via GW emission (Equation (25)).

Table 2
Model Parameters: Model Number, Star Cluster, Metallicity (Z), Primordial Binary Fraction of Massive Stars ( $f_{b,*}$ ), Spin Model, Initial Seed Mass ( $\mathcal{M}_{ini}$ ), Fraction of Models that Produce a BH More Massive than 500  $M_{\odot}$ , Fraction of Models that Produce a BH More Massive than 1000  $M_{\odot}$ 

Model	Star Cluster	$Z_{\mathrm{CL}}$	$f_{\mathrm{b},*}$	Spin Model	$\mathcal{M}_{ m ini}$ ( $M_{\odot}$ )	$f(\mathcal{M} > 100 M_{\odot})$	$f(\mathcal{M} > 500 M_{\odot})$	$f(\mathcal{M} > 800 M_{\odot})$
1	NSC	0.0001	0.0	Fuller & Ma (2019)	Stell. Evol.	$1.4 \times 10^{-1}$	$9.2 \times 10^{-3}$	$2.9 \times 10^{-3}$
1E	NSC	0.0001	0.0	Fuller & Ma (2019)	Stell. Evol.	$8.9 \times 10^{-2}$	$2.3 \times 10^{-3}$	$1.1 \times 10^{-3}$
2	NSC	0.001	0.0	Fuller & Ma (2019)	Stell. Evol.	$8.7 \times 10^{-2}$	$6.7 \times 10^{-3}$	$2.0 \times 10^{-3}$
3	NSC	0.01	0.0	Fuller & Ma (2019)	Stell. Evol.	$1.1 \times 10^{-2}$	$2.2 \times 10^{-4}$	0
4	NSC	0.0001	0.25	Fuller & Ma (2019)	Stell. Evol.	$1.4 \times 10^{-1}$	$9.9 \times 10^{-3}$	$4.8 \times 10^{-3}$
5	NSC	0.0001	0.5	Fuller & Ma (2019)	Stell. Evol.	$1.3 \times 10^{-1}$	$9.1 \times 10^{-3}$	$4.2 \times 10^{-3}$
6	NSC	0.0001	0.75	Fuller & Ma (2019)	Stell. Evol.	$1.3 \times 10^{-1}$	$9.5 \times 10^{-3}$	$3.9 \times 10^{-3}$
7	NSC	0.0001	1.0	Fuller & Ma (2019)	Stell. Evol.	$1.3 \times 10^{-1}$	$7.6 \times 10^{-3}$	$3.1 \times 10^{-3}$
8	NSC	0.0001	0.0	GENEVA	Stell. Evol.	$9.2 \times 10^{-3}$	0	0
9	NSC	0.0001	0.0	MESA	Stell. Evol.	$9.6 \times 10^{-2}$	$6.9 \times 10^{-3}$	$2.2 \times 10^{-3}$
10	NSC	0.0001	0.0	Fuller & Ma (2019)	50	$5.6 \times 10^{-1}$	$4.3 \times 10^{-2}$	$2.1 \times 10^{-2}$
11	NSC	0.0001	0.0	Fuller & Ma (2019)	100	1	$1.6 \times 10^{-1}$	$1.1 \times 10^{-1}$
12	NSC	0.0001	0.0	Fuller & Ma (2019)	150	1	$2.8 \times 10^{-1}$	$2.2 \times 10^{-1}$
13	NSC	0.0001	0.0	Fuller & Ma (2019)	200	1	$4.1 \times 10^{-1}$	$3.4 \times 10^{-1}$
14	GC	0.0001	0.0	Fuller & Ma (2019)	Stell. Evol.	$3.5 \times 10^{-2}$	0	0
15	GC	0.001	0.0	Fuller & Ma (2019)	Stell. Evol.	$1.5 \times 10^{-2}$	0	0
16	GC	0.01	0.0	Fuller & Ma (2019)	Stell. Evol.	0	0	0

- 6. We compute the recoil kick (Equation (26)) and the remnant spin and mass. If it is not ejected, we compute the timescale for the seed to sink back to the cluster center (Equation (15)).
- 7. If the seed is retained in the cluster and the total elapsed time is smaller than 10 Gyr, we repeat step (3) to again generate hierarchical mergers.

#### 3. Results

In this section, we study repeated mergers, the formation of IMBHs, and BHs in the mass gap in a population of NSCs.

We summarize in Table 2 the models we investigate in our simulations. We explore the role of the host cluster metallicity, primordial binary fraction in massive stars, and BH spin models. We also consider the case where the initial seed mass is fixed to four different mass values  $(50\,M_\odot,\,100\,M_\odot,\,150\,M_\odot,\,$  and  $200\,M_\odot$ ). Finally, we run three models where the host cluster mass and density are drawn from distributions that describe a population of GCs. In our simulations, we assume that spin orientations at merger are isotropic, as appropriate to merging binaries assembled in a dynamical environment. We integrate each simulation either up to 10 Gyr or until the growing seed is ejected from the host cluster, where further growth is quenched. Each result we present is the average over  $10^4$  model realizations.

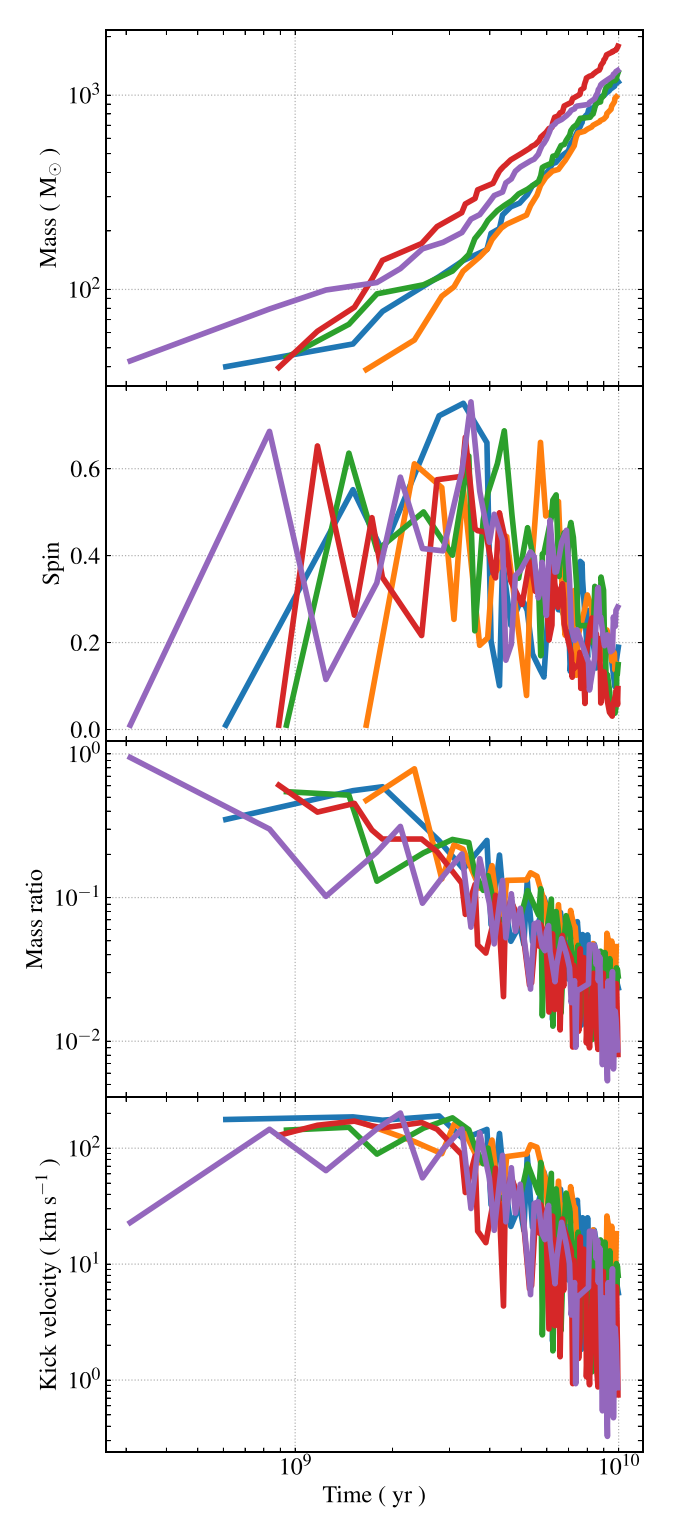
# 3.1. Formation of Intermediate-mass Black Holes

In Figure 1, we show an example of the growth of  $\sim 1000\,M_\odot$  IMBHs in Model 1, where we plot the mass evolution, the spin evolution, the mass ratio of mergers, and the recoil kick imparted to the merger remnant as a function of time. The trend in the recoil kick results from the fact that it depends both on the asymmetric mass ratio and on the spins of the progenitors (see Equation (26)), which we have set to zero in Model 1. As the BH seed merges with other BHs and increases its mass, the typical mass ratio decreases and so does the recoil kick imparted to the growing seed, which remains smaller than the escape speed of the host cluster, which is around  $200\,\mathrm{km\,s}^{-1}$  in these examples.

Concerning the spins, we confirm the previous results that found the spin of the growing seed decreases as a function of time or its growing mass (Antonini et al. 2019; Fragione & Silk 2020). The evolution of the seed spin is quite general, with the first merger producing a remnant with a dimensionless spin parameter of about 0.7 (starting from two slowly spinning BHs), which then tends to decrease with subsequent mergers. In Figure 2, we show the final BH spin as a function of its mass for Model 1. The spin of the BHs tends to decrease with the number of mergers, eventually producing a negative correlation between mass and spin. The reason is as follows. After the first mergers, the seed spin is about 0.7, if BHs are born slowly spinning. The angular momentum imparted to the growing seed during each merger is  $\propto m_2 \mathcal{M}$ , with the radius at the innermost stable circular orbit (ISCO)  $r_{\rm ISCO} \propto \mathcal{M}$ , which causes the spin parameter to change by  $\sim m_2/\mathcal{M}$ . Because at early times  $m_2$  can be comparable to  $\mathcal{M}$ , the initial variations in the remnant spins tend to be larger than the ones at late times when  $\mathcal{M} \gg m_2$ , as also seen in Figure 1. Assuming an isotropic geometry of BBH mergers as appropriate to a dynamical environment, the final inspiral and deposition of angular momentum happen at random angles to the previous spin axis of the growing seed. However, the growing seed undergoes a damped random walk in the evolution of its spin because retrograde orbits become unstable at a larger specific angular momentum than do prograde orbits, so it is easier to decrease than to increase the spin magnitude (Miller 2002; Hughes & Blandford 2003; Mandel et al. 2008). So the random walk takes the spin magnitude of the growing seed to small values eventually. Indeed, we find that BHs growing to a mass  $\gtrsim 1000 \, M_{\odot}$  have dimensionless spin parameters  $\leq 0.3$ .

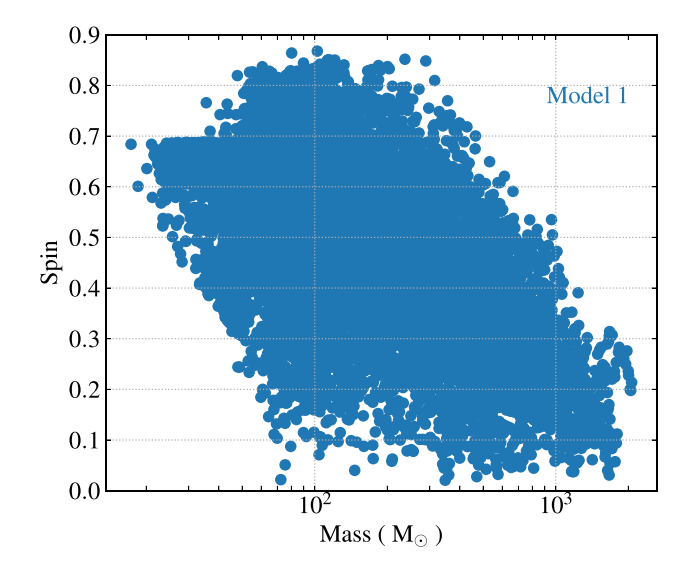
### 3.1.1. Effect of the Cluster Metallicity

Figure 3 shows the final BH mass (top) and spin (bottom) for different values of cluster metallicity (Models 1–3). In these models, the cluster primordial binary fraction of massive stars is set to  $f_{\rm b,*}=0$ , while BHs are assumed to be born nonspinning. The metallicity of the progenitors leaves an imprint on the mass spectrum as it impacts the typical cluster BH mass. We find that the maximum mass that the BH seed can reach is about  $1000\,M_\odot$  for solar metallicity and about  $3000\,M_\odot$  for  $Z_{\rm CL}=0.0001$  and



**Figure 1.** Example of growth of  $\sim 1000\,M_\odot$  IMBHs in Model 1. Different colors represent different formation histories. In order from the top: mass evolution, spin evolution, mass ratio of mergers, and recoil kick imparted to the merger remnant. In these examples, the escape speed of the host cluster is around 200 km s<sup>-1</sup>.

 $Z_{\rm CL} = 0.001$ . Moreover, the peak of the distributions tends to cluster around the maximum mass of the first-generation mergers, which is smaller for higher metallicities. On the other hand, we find that the host cluster metallicity has only a marginal effect on the spin spectrum.



**Figure 2.** Final spin of the growing BH seed as a function of its mass for Model 1. The spin of the BHs tends to decrease with the number of mergers (hence the BH mass), and a correlation exists between the mass and spin of the BHs.

We note that our considerations depend also on the details of the BH-mass spectrum. In our models, we have sampled the secondary mass in the range  $[m_{\min,BH}, m_{\max,BH}]$ , as appropriate to the BHmass spectrum at a metallicity  $Z_{CL}$ . To understand how our results depend on this assumption, we rerun Model 1, drawing the secondary masses in the range [ $m_{\min, \mathrm{BH}}, \ \mathcal{M}$ ] (as recently assumed in the models of Mapelli et al. 2021). This assumption might be justified by the fact that there might be more than one growing seed in a given cluster (Kremer et al. 2020a; González et al. 2021; Weatherford et al. 2021). While it might be reasonable at the beginning of the cluster evolution, this assumption becomes less justified when the seed mass grows to a few hundred solar masses. We illustrate the outcome of this additional run in Figure 3. We find that the main effect of this choice is to decrease by a factor of  $\sim$ 7 the relative abundance of seeds that grow to masses  $\gtrsim 500 \, M_{\odot}$ . This trend can be justified by the fact that secondaries can be as massive as  $\mathcal{M}$  during the whole cluster lifetime when sampling in the range  $[m_{\min, BH}, m_{\max, BH}]$ . As a result, the mass ratio can be as high as unity and the recoil kick can eject the growing BH seed. On the other hand, the ejection of the seed is quenched when sampling in the range  $[m_{\min,BH}, m_{\max,BH}]$ , as appropriate to the BH-mass spectrum at a metallicity  $Z_{CL}$ . In this case, the mass ratio becomes too small to lead to high recoil kicks after the seeds have grown to sufficiently high masses (Fragione & Silk 2020).

#### 3.1.2. Effect of Primordial Binary Fraction

In Models 4–7, we study the effect of the primordial binary fraction for massive stars. In these models, the cluster metallicity is fixed to  $Z_{\rm CL}=0.0001$ , and BHs are assumed to be born nonspinning, but the primordial binary fraction for massive stars is increased gradually all the way to  $f_{\rm b,*}=1$ . The main motivation is that bound stellar multiples are common, and surveys of massive stars, which are the progenitors of BHs, have shown that more than  $\sim 50\%$  have at least one or two stellar companions, respectively (e.g., Duquennoy & Mayor 1991; Raghavan et al. 2010; Sana et al. 2013; Sana 2017). We find that changing the primordial binary fractions of stars that are BH progenitors does not have a significant impact on the mass distribution or on the relative outcomes (see Table 2).

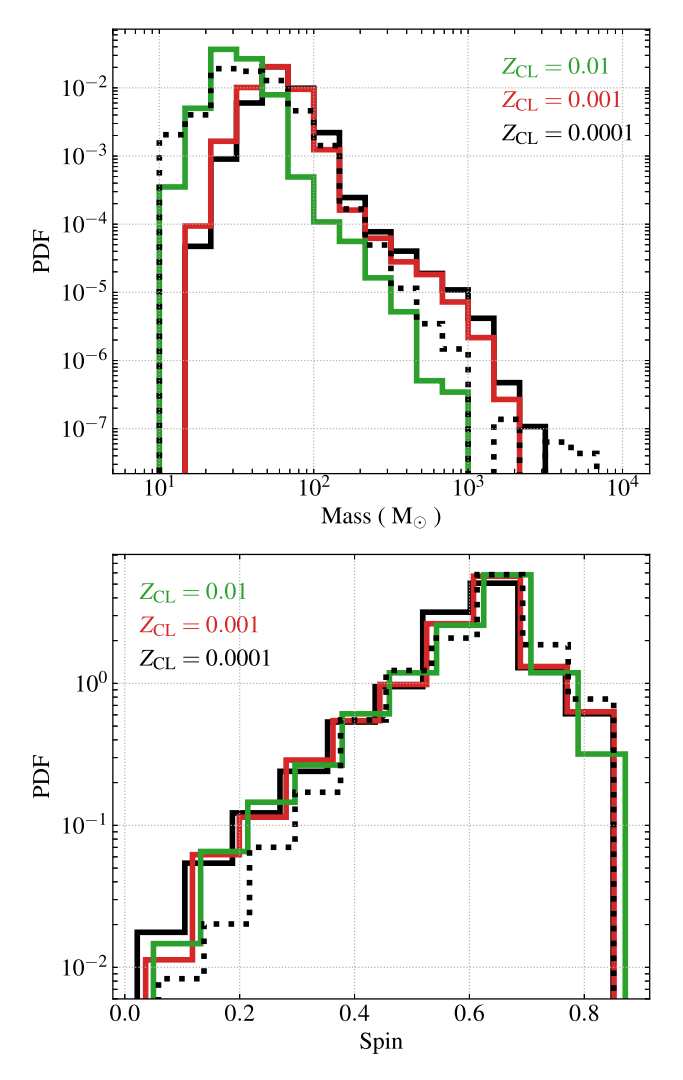


**Figure 3.** Final BH mass (top) and spin (bottom) for different values of cluster metallicity. The dotted black line represents results from Model 1 when the secondary BH masses are drawn in the range  $[m_{\min, BH}, \mathcal{M}]$ . The cluster primordial binary fraction of massive stars is set to  $f_{b,*} = 0$ , while BHs are assumed to be born nonspinning.

### 3.1.3. Effect of Black Hole Spin

In Models 8–9, we consider the impact of different assumptions on the BH spin at birth. In particular, we use the prescriptions of the GENEVA stellar evolution code (Eggenberger et al. 2008; Ekström et al. 2012) and the MESA stellar evolution code (Paxton et al. 2011, 2015) in Model 8 and Model 9, respectively. We show in Figure 4 the final BH mass for different prescriptions for BH spins at birth, compared to Model 1. The cluster metallicity is fixed to  $Z_{CL} = 0.0001$  and the primordial binary fraction of massive stars is set to  $f_{b,*} = 0$ . We find that, while Model 9 produces a mass spectrum that is consistent with the mass spectrum from Model 1, Model 8 does not produce BHs more massive than about  $200 M_{\odot}$ . The reason is that the GENEVA code predicts that most of the BHs form with a high spin, while the MESA code leads to BHs of all masses to form with a small residual spin,  $\sim 0.1.8$  Therefore, the recoil kicks after merger are typically larger than the cluster

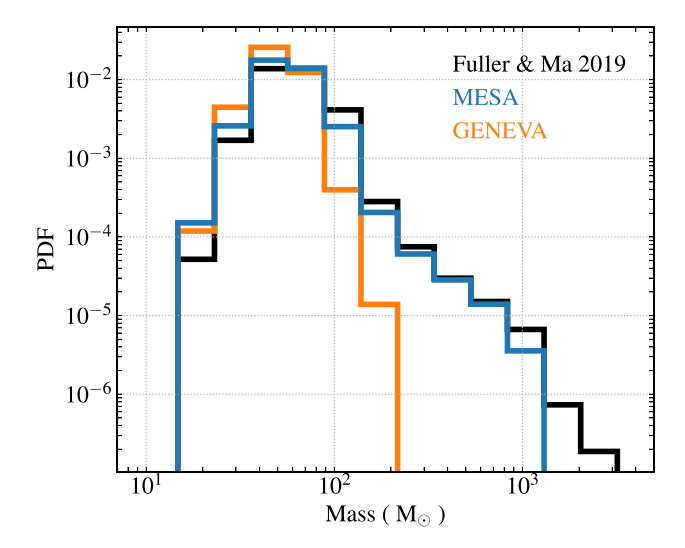


**Figure 4.** Final BH mass for different prescriptions for BH spins at birth in Models 8–9, compared to Model 1. The cluster metallicity is fixed to  $Z_{\rm CL} = 0.0001$ , and the primordial binary fraction of massive stars is set to  $f_{\rm b,*} = 0$ .

escape speed in Model 8, resulting in the ejection of the growing seed. Note also that while Model 9 produces a mass spectrum that is consistent with the mass spectrum from Model 1, the probability of forming massive BHs is about 1.5 times smaller than Model 1. The reason has again to be found in the typical BH spins, which are  $\sim 0.1$  in Model 9, while BHs are assumed to be born nonspinning in Model 1.

#### 3.1.4. Initial Seed Mass

In Models 10–13, we consider how the final BH mass depends on the initial seed mass  $\mathcal{M}_{\rm ini}$ . We assume that the growing seed has an initial mass of  $50\,M_\odot$ ,  $100\,M_\odot$ ,  $150\,M_\odot$ , and  $200\,M_\odot$ , respectively. In these models, the cluster metallicity is fixed to  $Z_{\rm CL}=0.0001$ , the primordial binary fraction of massive stars to is set to  $f_{\rm b,*}=0$ , and BHs are assumed to be born nonspinning. We show the results in Figure 5. We find that the larger the initial seed mass, the larger the final BH mass. Moreover, about 2%, 11%, 22%, and 34% of the runs produce a BH with final mass >  $1000\,M_\odot$  for  $\mathcal{M}_{\rm ini}=50\,M_\odot$ ,  $100\,M_\odot$ ,  $150\,M_\odot$ , and  $200\,M_\odot$ , respectively (see Table 2). Therefore, if clusters are born with a massive seed (e.g., Kremer et al. 2020a; González et al. 2021; Weatherford et al. 2021), they can grow efficiently to  $\gtrsim 10^3\,M_\odot$ .

#### 3.1.5. Cluster Evolution

In our approach, we have ignored the possible evolution of the global properties of the NSCs. While there is not a straightforward way to model the cosmic evolution of NSCs, we can adopt a simplified model (Model 1E in Table 2) similar to what is sometimes done for GCs, which experience a less complex evolution. Specifically, we follow Hénon's principle to model the global properties of a cluster and assume that the heating rate from BH binaries in the core has to balance the energy flow into the whole cluster (Hénon 1961). We model the heating rate of the star cluster as a function of time as (Gieles et al. 2011; Alexander & Gieles 2012; Antonini & Gieles 2020; Antonini et al. 2019)

This is because the GENEVA code does not include magnetic fields, so the core-to-envelope angular momentum transport is purely convective and, therefore, inefficient.

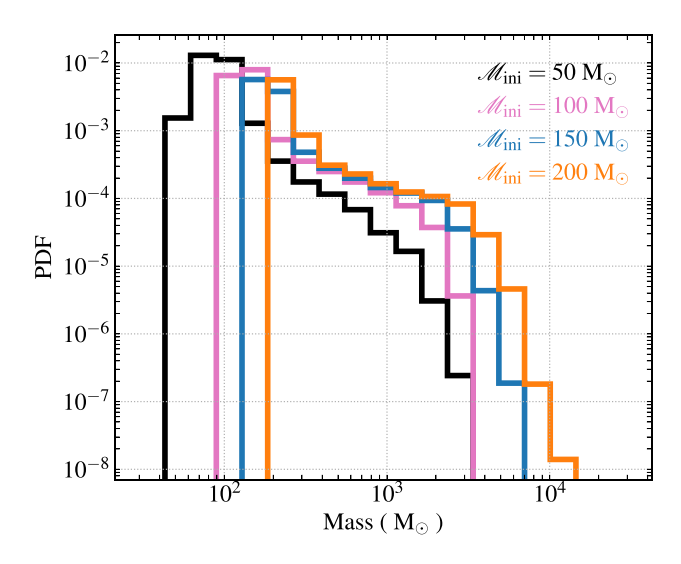


**Figure 5.** Final BH mass for different values of the initial seed mass in Models 10–13. The cluster metallicity is fixed to  $Z_{\rm CL}=0.0001$ , and the primordial binary fraction of massive stars is set to  $f_{\rm b,*}=0$ . BHs are assumed to be born nonspinning.

$$\dot{E}(t) = \dot{E}(0) \left( \frac{3}{2} \frac{\gamma t}{\tau_{\text{rh},0}} + 1 \right)^{-5/3}, \tag{32}$$

where  $\gamma \approx 0.1$  is a constant,

$$\dot{E}(0) = 2.3 \times 10^5 \, M_{\odot} (\text{ km s}^{-1})^2 \, \text{Myr}^{-1} \times \left(\frac{M_{\text{CL}}}{10^5 \, M_{\odot}}\right)^{2/3} \left(\frac{\rho_{\text{h}}}{10^5 \, M_{\odot} \, \text{pc}^{-3}}\right)^{5/6}, \tag{33}$$

 $\rho_{\rm h} = 3M_{\rm CL}/(8\pi r_{\rm h}^3)$  is the average density within the cluster half-mass radius, and  $\tau_{\rm rh,0}$  is the initial average relaxation timescale within  $r_{\rm h}$ ,

$$\tau_{\rm rh,0} = 7.5 \,\mathrm{Myr} \left( \frac{M_{\rm CL}}{10^5 \,M_{\odot}} \right) \left( \frac{10^5 \,M_{\odot} \,\mathrm{pc}^{-3}}{\rho_{\rm h}} \right)^{1/2}.$$
(34)

Hénon's principle imposes that the required heating rate of the cluster is balanced with the loss of energy from the BH binaries in the core, and we assume that the binary containing the growing seed dominates the heating at all times. Therefore, we require that  $\dot{E}_{\rm bin}(t) = -\dot{E}(t)$ , where  $\dot{E}_{\rm bin}(t)$  is the rate of energy loss from the binary. From the previous equation, it follows that the timescale during which the binary exists and dynamical interactions dominate the energy flow of the cluster is given by (Antonini et al. 2019)

$$\tau_{\text{bin}} = \frac{G\mathcal{M}m_2}{2\max(a_{\text{ej}}, a_{\text{GW}})\dot{E}(t)}.$$
 (35)

Again,  $\max(a_{\rm ej}, a_{\rm GW})$  (see Equations (21)–(22)) is the semimajor axis at which the hardening interactions stop as a result of either a merger or the ejection of the binary. Now,  $a_{\rm GW}$  is computed by requiring that the rate of energy loss due to dynamical hardening equals that due to GW radiation<sup>9</sup>

(Antonini et al. 2019):

$$a_{\rm GW} = 0.01 \left[ \frac{(\mathcal{M}m_2)^2 (\mathcal{M} + m_2)}{M_{\odot}^5} \frac{M_{\odot} (\text{km s}^{-1})^2 \text{Myr}^{-1}}{\dot{E}_{\rm bin}(t)} \right]^{1/5}.$$
(36)

From Equation (35), we estimate the timescale for the binary to shrink to  $\max(a_{ej}, a_{GW})$ ; if  $a_{ej} > a_{GW}$ , the binary is ejected from the cluster halting further growth, otherwise the merger happens in the cluster. Note that in this framework the escape velocity decreases as a function of time as the cluster evolves:

$$v_{\rm esc}(t) = v_{\rm esc,0} \left( \frac{3}{2} \frac{\gamma t}{\tau_{\rm rh,0}} + 1 \right)^{-1/3},$$
 (37)

where  $v_{\rm esc,0}$  is the initial escape velocity.

Figure 6 compares the final BH mass obtained in Model 1 to the same model when a model (Equation (32)) for cluster evolution is taken into account. We find that including cluster evolution does not change significantly our results for masses  $\lesssim 100\,M_\odot$ . On the other hand, the likelihood of producing a BH with a final mass of  $\gtrsim 100\,M_\odot$  decreases by a factor of a few (see Table 2), owing to a typically longer binary heating rate (with respect to the binary shrinking rate computed with no cluster evolution) and decreasing cluster escape velocity.

#### 3.2. Black Holes in the Mass Gap

Here we show how our semianalytical framework predicts BH mergers in the mass gap. As an example, we explore the possibility that a system like GW190521 formed through multiple mergers. We show in Figure 7 (top panel) the mass of the secondary versus primary component of binary BH mergers in Model 1, when the secondary BH masses are drawn from the range  $[m_{\min}]_{BH}$ ,  $\mathcal{M}$ ]. This assumption is important because the maximum BH mass, even at low metallicity, is around  $50 M_{\odot}$ in our models, which requires the secondary of GW190521 to be the product of a previous merger as well (e.g., Fragione et al. 2020; Kimball et al. 2020, 2021; Mapelli et al. 2021). We also show the estimated component masses of GW190521 (Abbott et al. 2020a). Our results confirm that repeated mergers in dense star clusters are able to match the component masses of GW190521. Recently, Nitz & Capano (2021) reanalyzed the data of the LVK collaboration with a new waveform allowing for more extreme mass ratios and found that GW190521 is consistent with an intermediate-mass ratio inspiral with primary mass  $168^{+15}_{-61}\,M_{\odot}$  and secondary mass  $16^{+33}_{-3}\,M_{\odot}$  (see also Mehta et al. 2021). In this case, the primary mass is not inside the mass gap, but it is in the IMBH regime, while the secondary mass could be an ordinary (first-generation) stellar BH. As we show in the bottom panel of Figure 7, GW190521 would then be more consistent with Model 1 when the secondary BH masses are drawn in the range  $[m_{\min,BH}, m_{\max,BH}]$ , as appropriate to the cluster metallicity  $Z_{CL}$ .

# 3.3. Globular Clusters

For comparison, Models 14–16 represent GCs as host star clusters. For these models we draw the total masses from a lognormal distribution with mean  $\langle \log_{10}(M_{\rm CL}/M_{\odot}) \rangle = 5.3$  and standard deviation 0.4 (Harris 1996). Following Gnedin et al.

Note that we are ignoring the factor of  $(1 - e_{\rm BH})^{-7/10}$ , which is of order unity.

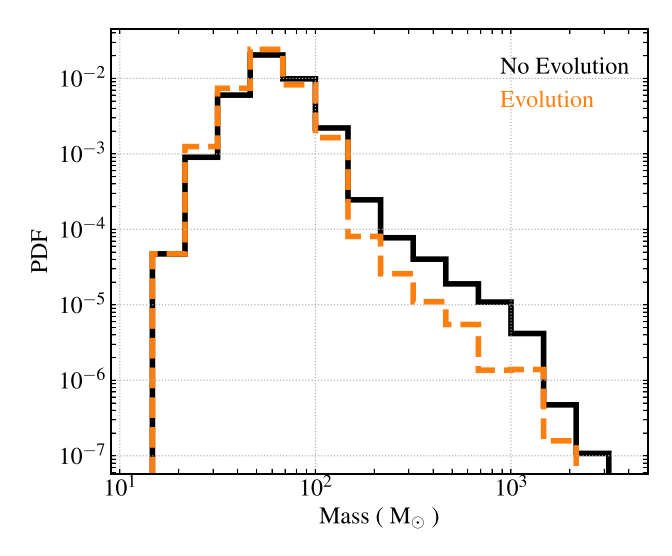


**Figure 6.** Final BH mass in Models 1 without (black solid) and with (orange dashed) cluster evolution. The cluster metallicity is fixed to  $Z_{\rm CL}=0.01$ , and the primordial binary fraction of massive stars is set to  $f_{\rm b,*}=0$ , while BHs are assumed to be born nonspinning.

(2014), we adopt the average density at the half-mass radius

$$\rho_{\rm h} = \begin{cases} 10^3 \, M_{\odot} \, \, \mathrm{pc}^{-3} & \text{for } M \leqslant 10^5 \, M_{\odot} \\ 10^3 \left(\frac{M}{10^5 \, M_{\odot}}\right)^2 \, M_{\odot} \, \, \mathrm{pc}^{-3} & \text{for } 10^5 \, M_{\odot} < M < 10^6 \, M_{\odot} \\ 10^5 \, M_{\odot} \, \, \mathrm{pc}^{-3} & \text{for } M \geqslant 10^6 \, M_{\odot}. \end{cases}$$
(38)

The above equation limits  $\rho_{\rm h}$  to  $10^5\,M_{\odot}\,{\rm pc}^{-3}$  in the most massive clusters, which is about the highest observed half-mass density. The cluster primordial binary fraction for massive stars is set to  $f_{\rm b,*}=0$ , while BHs are assumed to be born nonspinning.

We show the final BH mass for different values of the cluster metallicity for GCs in Figure 8 and compare to the results from Models 1–3. We find that only about 3% and 2% of the runs produce a BH more massive than  $100\,M_\odot$  for  $Z_{\rm CL}=0.0001$  and 0.001, while none in the case of solar metallicity (see Table 2). The reason is of course that GCs have lower escape speeds compared to NSCs and the recoil kick can eject the growing seed easily, halting further growth.

#### 4. Discussion and Conclusions

Our methodology is based on some approximations and assumptions. We discuss them in the following section and conclude with a brief summary of our main results.

# 4.1. Caveats against and Improvements in Current Methodology

In our models, we have sampled the masses and half-mass radii of NSCs from Equations (8)–(9), which are calibrated over observations of NSCs in the local universe (Georgiev et al. 2016). We have assumed that these properties have not evolved during the lifetime of a given NSC. However, star clusters expand as a consequence of two-body relaxation and lose mass (and expand) as a result of dynamical ejections and stellar evolution. For example, the fraction of mass in stars that turn into BHs is about

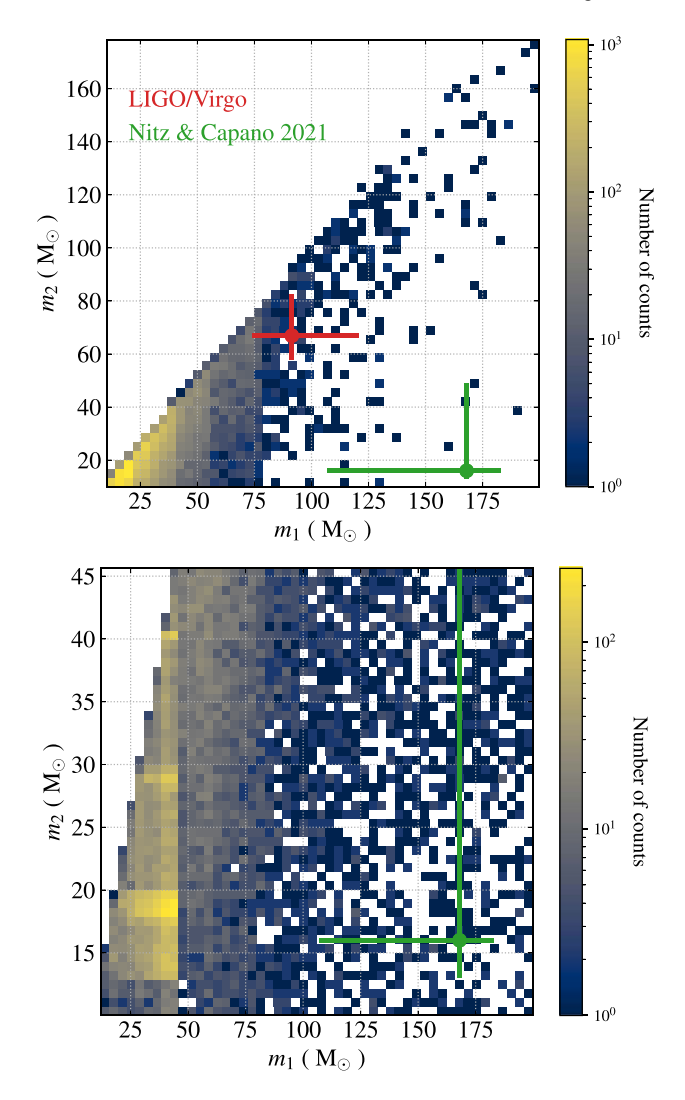


**Figure 7.** Mass of the secondary vs. primary component of BBH mergers in Model 1, when the secondary BH masses are drawn from the range  $[m_{\min, BH}, \mathcal{M}]$  (top) and the range  $[m_{\min, BH}, m_{\max, BH}]$  (bottom). We also report the estimated component masses of GW190521 from the LVK collaboration (Abbott et al. 2020a) and from Nitz & Capano (2021).

11% for a canonical (Kroupa 2001) IMF. For low metallicities, about two-thirds of the progenitor mass will be lost during stellar evolution, while this fraction is about nine-tenths for solar metallicity (e.g., see Figure 1 in Fragione et al. 2020). Therefore, a given cluster will lose about 7% and 10% of its initial mass for low and solar metallicities, respectively, when BH progenitors collapse and form BHs. This mass loss (along with the mass lost by other stars) will cause the star cluster to expand during its lifetime. Cluster expansion tends to lower the cluster mass and density, which in turn could prevent the growth of a massive seed (e.g., Antonini et al. 2019). However, episodes of core collapse and of gravothermal oscillations could temporarily increase the central density, which could result in an enhancement of the growth of the BH seed (e.g., Breen & Heggie 2013). Therefore, the overall effect of including the evolution of the NSC is difficult to predict.

While the previous discussion essentially assumes that an NSC is isolated, other important factors could be relevant to place a population of NSCs in the proper galactic and cosmological context. For example, we do not model the evolution of NSCs

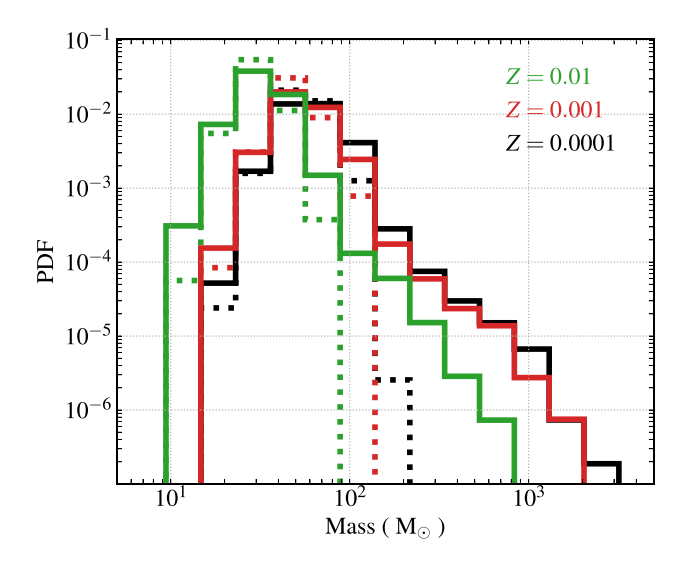


**Figure 8.** Final BH mass for different values of the cluster metallicity for NSCs (solid) from Models 1–3 and GCs (dotted) from Models 14–16. The primordial binary fraction in massive stars is set to  $f_{\rm b,*}=0$ , while BHs are assumed to be born nonspinning.

using an N-body approach, as this is computationally expensive and beyond what current codes can handle (e.g., Aarseth 2003; Giersz 2006; Rodriguez et al. 2022). While there is not a straightforward way to model the cosmic evolution of NSCs, various simplified models could be adopted (Gieles et al. 2011; Antonini et al. 2019). However, NSCs are not isolated environments on a cosmological scale; as there can be a continuous supply of stars and gas from the rest of the galaxy (e.g., Vogelsberger et al. 2014), there could be ongoing star formation and accretion of smaller star clusters (e.g., Antonini 2014), and SMBHs could be delivered to this region following galaxy collisions (e.g., Begelman et al. 1980). Note also that the NSC evolution could be significantly affected by the presence of an (single or binary) SMBH, especially if SMBH seeds are formed via direct collapse in the early universe. For example, SMBHs tend to create a cusp of stars and compact objects (e.g., Bahcall & Wolf 1976; Hopman & Alexander 2006; Alexander 2017; Fragione & Sari 2018) and could accrete gas (e.g., Kroupa et al. 2020; Natarajan 2021), with an AGN component that could be complementary in some cases (Tagawa et al. 2021c).

Finally, we note that we have not included star-star collisions and stellar runaway mergers. These processes could play a role because a massive BH seed could form from the collapse of a very massive star and, eventually, further accretion (e.g., Portegies Zwart & McMillan 2002; Inayoshi et al. 2020; Kremer et al. 2020a; Tagawa et al. 2020b; Di Carlo et al. 2021). These processes could possibly be enhanced in the case of a large primordial binary fraction of massive stars (González et al. 2021) and in the case of a top-heavy initial mass function (Weatherford et al. 2021). Tidal captures of stars may also lead to the formation of a massive BH (Stone et al. 2017a). For the typical masses and sizes of the NSCs in our sample, the timescales for this process and repeated mergers could be comparable. However, the tidal capture process relies on the assumption that a few BHs lurk in the core, which might not be the case because the BH-burning process, which ejects most of the cluster BHs, could last more than a Hubble time for a typical NSC (e.g., Kremer et al. 2020b).

Despite all of the above limitations, our model gives general scenarios for the formation of massive BHs through repeated mergers in dense star clusters and the population of ejected BHs (see also Fragione & Silk 2020). Importantly, we have drawn masses and half-mass radii of NSCs consistently with observations (Georgiev et al. 2016), weighting their abundances using the distribution of galaxies in the local universe (Furlong et al. 2015). This procedure is crucial to ensure the correct sampling and correlation of the distributions of NSC parameters because their masses and sizes are closely related. While our analysis still lacks a detailed prescription for the evolution of the background cluster, we have included some treatment of our dense star clusters as a multizone model, using the three-parameter potential-density pair of Stone & Ostriker (2015).

We have fully integrated for the first time a (single and binary) stellar evolution code with the underlying dynamical model. We note that our current stellar evolutionary code includes the most up-to-date prescriptions for stellar winds and remnant formation (Banerjee et al. 2020). This allows us to compute a realistic BH-mass spectrum for any cluster metallicity and to determine BH spins at birth from fits to stellar tracks (Eggenberger et al. 2008; Paxton et al. 2011, 2015; Ekström et al. 2012). Both the distributions of initial BH masses and spins are fundamental to determine if a massive seed can grow as a result of hierarchical mergers. For the sake of versatility, our method also includes the possibility of including an initial BH seed (with a given spin), which might be the end product of a very massive star formed via stellar mergers (e.g., Portegies Zwart & McMillan 2002; Kremer et al. 2020a; Di Carlo et al. 2021; González et al. 2021).

Finally, we note that our scheme still lacks the time evolution of the BH-mass spectrum, which can be modified over time by the dynamical ejection of BHs. Also, we take into account only mergers between our growing seed and first-generation BHs, ignoring the possible contributions of secondaries from a previous merger. Finally, we assume that our processes take place after an average timescale, which could be in principle be replaced by direct integration of the few-body interaction continuously experienced by the growing seed. We leave the detailed exploration and implementation of each of these improvements to future work.

#### 4.2. Summary

The mass spectrum of BHs is among the most hotly debated topics in modern astrophysics. Current stellar evolution models predict a dearth of BHs with masses  $\gtrsim 50\,M_\odot$  and, even though the LVK collaboration has detected almost 50 BBHs, the exact shape of the BH-mass spectrum remains a mystery.

In this paper, we have presented a semianalytic framework to investigate hierarchical mergers in dense star clusters, expanding upon the method originally developed in Fragione & Silk (2020). Our method allows us to rapidly study the outcomes of hierarchical mergers in dense star clusters and probe how they are affected by the cluster masses, densities, metallicities, and primordial binary fractions and by the different assumptions on the BH-mass spectrum and spins.

We have studied repeated mergers, BHs in the mass gap, and the formation of IMBHs in a population of NSCs. We have shown that a BH seed can grow up to  $\sim 10^3 \, M_{\odot} - 10^4 \, M_{\odot}$  as a result of repeated mergers with stellar BHs. We have found that the smaller the cluster metallicity, the larger is the typical final BH mass. Moreover, we have confirmed that the spin of the

BHs tends to decrease with the number of mergers and, as a result, more massive BHs have typically smaller spins. We have also found that the primordial binary fraction in massive stars does not have a significant impact on our results, while the choice of the BH spin model is crucial, with low birth spins leading to the production of a larger population of massive BHs. We have also illustrated that GW190521 can be born as a result of hierarchical mergers in an NSC. Finally, we have discussed that, unlike NSCs, GCs are not massive and dense enough to retain the merger remnant after a recoil kick is imparted, and a BH seed cannot grow significantly in mass via repeated mergers with other BHs.

We thank Sambaran Banerjee for useful discussions on stellar evolutionary codes and for updating SSE and BSE with state-of-the-art prescriptions. G.F. and F.A.R. acknowledge support from NASA Grant 80NSSC21K1722. This work received funding from the European Research Council (ERC) under the European Union's Horizon 2020 Programme for Research and Innovation ERC-2014-STG under grant agreement No. 638435 (GalNUC) (to B.K.).

#### ORCID iDs

Giacomo Fragione https://orcid.org/0000-0002-7330-027X Bence Kocsis https://orcid.org/0000-0002-4865-7517 Frederic A. Rasio https://orcid.org/0000-0002-7132-418X Joseph Silk https://orcid.org/0000-0002-1566-8148

#### References

```
Aarseth, S. J. 2003, Gravitational N-Body Simulations (Cambridge: Cambridge
   Univ. Press), 430
Abbott, B. P., Abbott, R., Abbott, T. D., et al. 2019, PhRvX, 9, 031040
Abbott, R., Abbott, T. D., Abraham, S., et al. 2020a, arXiv:2010.14527
Abbott, R., Abbott, T. D., Abraham, S., et al. 2020b, arXiv:2010.14533
Abbott, R., Abbott, T. D., Abraham, S., et al. 2020c, arXiv:2010.14529
Alexander, P. E. R., & Gieles, M. 2012, MNRAS, 422, 3415
Alexander, T. 2017, ARA&A, 55, 17
Antonini, F. 2014, ApJ, 794, 106
Antonini, F., & Gieles, M. 2020, PhRvD, 102, 123016
Antonini, F., Gieles, M., & Gualandris, A. 2019, MNRAS, 486, 5008
Antonini, F., & Perets, H. B. 2012, ApJ, 757, 27
Antonini, F., & Rasio, F. A. 2016, ApJ, 831, 187
Arca Sedda, M., Mapelli, M., Spera, M., et al. 2020, ApJ, 894, 133
Arca-Sedda, M., & Gualandris, A. 2018, MNRAS, 477, 4423
Arca-Sedda, M., Li, G., & Kocsis, B. 2021, A&A, 650, A189
Askar, A., Szkudlarek, M., Gondek-Rosińska, D., Giersz, M., & Bulik, T.
   2017, MNRAS, 464, L36
Bahcall, J. N., & Wolf, R. A. 1976, ApJ, 209, 214
Baibhav, V., Berti, E., Gerosa, D., et al. 2021, PRvD, 104, 084002
Baibhav, V., Gerosa, D., Berti, E., et al. 2020, PhRvD, 102, 043002
Banerjee, S. 2018, MNRAS, 473, 909
Banerjee, S., Belczynski, K., Fryer, C. L., et al. 2020, A&A, 639, A41
Bartos, I., Kocsis, B., Haiman, Z., & Márka, S. 2017, ApJ, 835, 165
Bavera, S. S., Fragos, T., Zevin, M., et al. 2021, A&A, 647, A153
Begelman, M. C., Blandford, R. D., & Rees, M. J. 1980, Natur, 287, 307
Belczynski, K., Hirschi, R., Kaiser, E. A., et al. 2020, ApJ, 890, 113
Belczynski, K., Holz, D. E., Bulik, T., & O'Shaughnessy, R. 2016, Natur,
   534, 512
Breen, P. G., & Heggie, D. C. 2013, MNRAS, 432, 2779
Breivik, K., Coughlin, S., Zevin, M., et al. 2020, ApJ, 898, 71
Chandrasekhar, S. 1943, ApJ, 97, 255
Choksi, N., Volonteri, M., Colpi, M., et al. 2019, ApJ, 873, 100
Chruslinska, M., Belczynski, K., Klencki, J., & Benacquista, M. 2018,
          S, 474, 2937
de Mink, S. E., & Mandel, I. 2016, MNRAS, 460, 3545
Di Carlo, U. N., Mapelli, M., Giacobbo, N., et al. 2020, MNRAS, 498, 495
Di Carlo, U. N., Mapelli, M., Pasquato, M., et al. 2021, MNRAS, 507, 5132
Dominik, M., Belczynski, K., Fryer, C., et al. 2013, ApJ, 779, 72
```

```
Duchêne, G., & Kraus, A. 2013, ARA&A, 51, 269
Duquennoy, A., & Mayor, M. 1991, A&A, 248, 485
Eggenberger, P., Meynet, G., Maeder, A., et al. 2008, Ap&SS, 316, 43
Ekström, S., Georgy, C., Eggenberger, P., et al. 2012, A&A, 537, A146
Fragione, G., & Banerjee, S. 2020, ApJL, 901, L16
Fragione, G., Grishin, E., Leigh, N. W. C., Perets, H. B., & Perna, R. 2019a,
   MNRAS, 488, 47
Fragione, G., & Kocsis, B. 2018, PhRvL, 121, 161103
Fragione, G., & Kocsis, B. 2019, MNRAS, 486, 4781
Fragione, G., Leigh, N. W. C., & Perna, R. 2019b, MNRAS, 488, 2825
Fragione, G., & Loeb, A. 2021, MNRAS, 502, 3879
Fragione, G., Loeb, A., & Rasio, F. A. 2020, ApJL, 902, L26
Fragione, G., & Sari, R. 2018, ApJ, 852, 51
Fragione, G., & Silk, J. 2020, MNRAS, 498, 4591
Fryer, C. L., & Kalogera, V. 2001, ApJ, 554, 548
Fuller, J., & Ma, L. 2019, ApJL, 881, L1
Furlong, M., Bower, R. G., Theuns, T., et al. 2015, MNRAS, 450, 4486
Georgiev, I. Y., & Böker, T. 2014, MNRAS, 441, 3570
Georgiev, I. Y., Böker, T., Leigh, N., Lützgendorf, N., & Neumayer, N. 2016,
           , 457, 2122
Giacobbo, N., & Mapelli, M. 2018, MNRAS, 480, 2011
Gieles, M., Heggie, D. C., & Zhao, H. 2011, MNRAS, 413, 2509
Giersz, M. 2006, MNRAS, 371, 484
Gnedin, O. Y., Ostriker, J. P., & Tremaine, S. 2014, ApJ, 785, 71
Gondán, L., & Kocsis, B. 2021, MNRAS, 506, 1665
Gondán, L., Kocsis, B., Raffai, P., & Frei, Z. 2018, ApJ, 860, 5
González, E., Kremer, K., Chatterjee, S., et al. 2021, ApJL, 908, L29
González, J. A., Sperhake, U., Brügmann, B., Hannam, M., & Husa, S. 2007,
   PhRvL, 98, 091101
Grishin, E., Perets, H. B., & Fragione, G. 2018, MNRAS, 481, 4907
Gültekin, K., Miller, M. C., & Hamilton, D. P. 2004, ApJ, 616, 221
Hamers, A. S., Bar-Or, B., Petrovich, C., & Antonini, F. 2018, ApJ, 865, 2
Hamers, A. S., Fragione, G., Neunteufel, P., & Kocsis, B. 2021, MNRAS,
Hamers, A. S., & Samsing, J. 2019, MNRAS, 487, 5630
Harris, W. E. 1996, AJ, 112, 1487
Heger, A., Fryer, C. L., Woosley, S. E., Langer, N., & Hartmann, D. H. 2003,
    nJ. 591, 288
Heggie, D. C. 1975, MNRAS, 173, 729
Hénon, M. 1961, AnAp, 24, 369
Hoang, B.-M., Naoz, S., Kocsis, B., et al. 2018, ApJ, 856, 140
Hobbs, G., Lorimer, D. R., Lyne, A. G., & Kramer, M. 2005, MNRAS,
Hofmann, F., Barausse, E., & Rezzolla, L. 2016, ApJL, 825, L19
Hopman, C., & Alexander, T. 2006, ApJL, 645, L133
Hughes, S. A., & Blandford, R. D. 2003, ApJL, 585, L101
Hurley, J. R., Pols, O. R., & Tout, C. A. 2000, MNRAS, 315, 543
Hurley, J. R., Tout, C. A., & Pols, O. R. 2002, MNRAS, 329, 897
Inayoshi, K., Visbal, E., & Haiman, Z. 2020, ARA&A, 58, 27
Jeans, J. H. 1919, MNRAS, 79, 408
Jiménez-Forteza, X., Keitel, D., Husa, S., et al. 2017, PhRvD, 95, 064024
Kimball, C., Talbot, C., Berry, C. P. L., et al. 2020, ApJ, 900, 177
Kimball, C., Talbot, C., Berry, C. P. L., et al. 2021, ApJL, 915, L35
Kobulnicky, H. A., Kiminki, D. C., Lundquist, M. J., et al. 2014, ApJS, 213, 34
Kremer, K., Chatterjee, S., Breivik, K., et al. 2018, PhRvL, 120, 191103
Kremer, K., Rodriguez, C. L., Amaro-Seoane, P., et al. 2019, PhRvD, 99,
Kremer, K., Spera, M., Becker, D., et al. 2020a, ApJ, 903, 45
Kremer, K., Ye, C. S., Rui, N. Z., et al. 2020b, ApJS, 247, 48
Kroupa, P. 2001, MNRAS, 322, 231
Kroupa, P., Subr, L., Jerabkova, T., & Wang, L. 2020, MNRAS, 498, 5652
Lee, H. M. 1995, MNRAS, 272, 605
Limongi, M., & Chieffi, A. 2018, ApJS, 237, 13
Liu, B., & Lai, D. 2018, ApJ, 863, 68
Liu, B., & Lai, D. 2019, MNRAS, 483, 4060
Liu, B., Lai, D., & Wang, Y.-H. 2019, ApJL, 883, L7
Lousto, C. O., Campanelli, M., Zlochower, Y., & Nakano, H. 2010, CQGra,
  27, 114006
Lousto, C. O., & Zlochower, Y. 2008, PhRvD, 77, 044028
Lousto, C. O., & Zlochower, Y. 2011, PhRvL, 107, 231102
Lousto, C. O., Zlochower, Y., Dotti, M., & Volonteri, M. 2012, PhRvD, 85,
Mandel, I., Brown, D. A., Gair, J. R., & Miller, M. C. 2008, ApJ, 681, 1431
Mapelli, M., Dall'Amico, M., Bouffanais, Y., et al. 2021, MNRAS, 505, 339
Martinez, M. A. S., Fragione, G., Kremer, K., et al. 2020, ApJ, 903, 67
Martinez, M. A. S., Rodriguez, C. L., & Fragione, G. 2021, arXiv:2105.01671
```

```
McKernan, B., Ford, K. E. S., & O'Shaughnessy, R. 2020, arXiv:2002.00046
Mehta, A. K., Buonanno, A., Gair, J., et al. 2021, arXiv:2105.06366
Miller, M. C. 2002, ApJ, 581, 438
Miller, M. C., & Hamilton, D. P. 2002, MNRAS, 330, 232
Miller, M. C., & Lauburg, V. M. 2009, ApJ, 692, 917
Morscher, M., Pattabiraman, B., Rodriguez, C., Rasio, F. A., & Umbreit, S.
   2015, ApJ, 800, 9
Natarajan, P. 2021, MNRAS, 501, 1413
Nitz, A. H., & Capano, C. D. 2021, ApJL, 907, L9
O'Leary, R. M., Kocsis, B., & Loeb, A. 2009, MNRAS, 395, 2127
O'Leary, R. M., Meiron, Y., & Kocsis, B. 2016, ApJL, 824, L12
Pattabiraman, B., Umbreit, S., Liao, W.-K., et al. 2013, ApJS, 204, 15
Paxton, B., Bildsten, L., Dotter, A., et al. 2011, ApJS, 192, 3
Paxton, B., Marchant, P., Schwab, J., et al. 2015, ApJS, 220, 15
Perna, R., Wang, Y.-H., Farr, W. M., Leigh, N., & Cantiello, M. 2019, ApJL,
   878, L1
Peters, P. C. 1964, PhRv, 136, 1224
Petrovich, C., & Antonini, F. 2017, ApJ, 846, 146
Portegies Zwart, S. F., & McMillan, S. L. W. 2000, ApJL, 528, L17
Portegies Zwart, S. F., & McMillan, S. L. W. 2002, ApJ, 576, 899
Quinlan, G. D. 1996, NewA, 1, 35
Raghavan, D., McAlister, H. A., Todd, J., et al. 2010, ApJS, 190, 1
Rasskazov, A., & Kocsis, B. 2019, ApJ, 881, 20
Rastello, S., Amaro-Seoane, P., Arca-Sedda, M., et al. 2019, MNRAS,
  483, 1233
Renzo, M., Farmer, R., Justham, S., et al. 2020, A&A, 640, A56
Rodriguez, C. L., Amaro-Seoane, P., Chatterjee, S., & Rasio, F. A. 2018,
   PhRvL, 120, 151101
Rodriguez, C. L., & Antonini, F. 2018, ApJ, 863, 7
Rodriguez, C. L., Kremer, K., Grudić, M. Y., et al. 2020, ApJL, 896, L10
Rodriguez, C. L., Weatherford, N. C., Coughlin, S. C., et al. 2022, ApJS,
   258, 22
Rossa, J., van der Marel, R. P., Böker, T., et al. 2006, AJ, 132, 1074
Samsing, J., Askar, A., & Giersz, M. 2018, ApJ, 855, 124
Sana, H., de Koter, A., de Mink, S. E., et al. 2017, in IAU Symp. 329, The
   Lives and Death-Throes of Massive Stars, ed. J. J. Eldridge et al.
   (Cambridge: Cambridge Univ. Press), 110
```

```
Sana, H., de Mink, S. E., de Koter, A., et al. 2012, Sci, 337, 444
Sana, H., et al. 2013, A&A, 550, A107
Santoliquido, F., Mapelli, M., Giacobbo, N., et al. 2021, MNRAS,
  502, 4877
Seth, A. C., Dalcanton, J. J., Hodge, P. W., & Debattista, V. P. 2006, AJ,
  132, 2539
Spera, M., & Mapelli, M. 2017, MNRAS, 470, 4739
Spera, M., Mapelli, M., Giacobbo, N., et al. 2019, MNRAS, 485, 889
Stone, N. C., Küpper, A. H. W., & Ostriker, J. P. 2017a, MNRAS,
  467, 4180
Stone, N. C., Metzger, B. D., & Haiman, Z. 2017b, MNRAS, 464, 946
Stone, N. C., & Ostriker, J. P. 2015, ApJL, 806, L28
Su, Y., Liu, B., & Lai, D. 2021, MNRAS, 505, 3681
Tagawa, H., Haiman, Z., Bartos, I., Kocsis, B., & Omukai, K. 2021a, MNRAS,
  507, 3362
Tagawa, H., Haiman, Z., & Kocsis, B. 2020a, ApJ, 898, 25
Tagawa, H., Haiman, Z., & Kocsis, B. 2020b, ApJ, 892, 36
Tagawa, H., Kocsis, B., Haiman, Z., et al. 2021b, ApJL, 907, L20
Tagawa, H., Kocsis, B., Haiman, Z., et al. 2021c, ApJ, 908, 194
Tanikawa, A., Kinugawa, T., Yoshida, T., et al. 2021, MNRAS, arXiv:2010.
  07616
The LIGO Scientific Collaboration, & the Virgo Collaboration 2020a,
  arXiv:2009.01075
The LIGO Scientific Collaboration, & the Virgo Collaboration 2020b, ApJL,
  900, L13
Varma, V., Gerosa, D., Stein, L. C., et al. 2019, PhRvL, 122, 011101
Vink, J. S., Higgins, E. R., Sander, A. A. C., & Sabhahit, G. N. 2021, MNRAS,
  504, 146
Vogelsberger, M., Genel, S., Springel, V., et al. 2014, MNRAS, 444,
  1518
Wang, H., Stephan, A. P., Naoz, S., et al. 2021, ApJ, 917, 76
Weatherford, N. C., Fragione, G., Kremer, K., et al. 2021, ApJL,
  907, L25
Wong, K. W. K., Breivik, K., Kremer, K., & Callister, T. 2021, PhRvD, 103,
Woosley, S. E. 2017, ApJ, 836, 244
Zevin, M., Bavera, S. S., Berry, C. P. L., et al. 2021, ApJ, 910, 152
```